Combined catalytic partial oxidation and CO_2 reforming of methane over supported cobalt catalysts

E. Ruckenstein * and H.Y. Wang

Department of Chemical Engineering, State University of New York at Buffalo, Amherst, NY 14260, USA
E-mail: feaeliru@acsu.buffalo.edu

Received 9 January 2001; accepted 12 February 2001

The combined partial oxidation and CO_2 reforming of methane to synthesis gas was investigated over the reduced Co/MgO, Co/CaO, and Co/SiO_2 catalysts. Only Co/MgO has proved to be a highly efficient and stable catalyst. It provided about 94–95% yields to H_2 and CO at the high space velocity of 105 000 ml g^{-1} h^{-1} and for feed ratios $CH_4/CO_2/O_2 = 4/2/1$, without any deactivation for a period of study of 110 h. In contrast, the reduced Co/CaO and Co/SiO_2 provided no activity for the formation of H_2 and CO. The structure and reducibility of the calcined catalysts were examined using X-ray diffraction and temperature-programmed reduction, respectively. A solid solution of CoO and MgO, which was difficult to reduce, was identified in the 800 °C calcined MgO-supported catalyst. The strong interactions induced by the formation of the solid solution are responsible for its superior activity in the combined reaction. The effects of reaction temperature, space velocity, and O_2/CO_2 ratio in the feed gases (while keeping the C/O ratio constant at 1/1) were investigated over the Co/MgO catalyst. The H_2/CO ratio in the product of the combined reaction increased with increasing O_2/CO_2 ratio in the feed.

KEY WORDS: combined partial oxidation and CO_2 reforming of methane; synthesis gas; Co catalyst

1. Introduction

The synthesis gas (a mixture of H_2 and CO) is a versatile feedstock for the methanol and Fischer–Tropsch syntheses and several other carbonylation, hydrogenation and reduction reactions. The currently employed steam reforming process (reaction (1)) is highly endothermic and provides a synthesis gas with a too high H_2/CO ratio (>3) [1,2]. In recent years, major research efforts have been concentrated on the CO_2 reforming (reaction (2)) [3–12] and the partial oxidation (reaction (3)) [13–23]. Like the steam reforming, the "dry" CO_2 reforming is also highly endothermic requiring a large energy input, while the partial oxidation is mildly exothermic with potential hazards due to the presence of hot spots [24,25].

$$CH_4 + H_2O \rightarrow CO + 3H_2 \qquad \Delta H^0_{298} = 206\ \text{kJ mol}^{-1}, \tag{1}$$

$$CH_4 + CO_2 \rightarrow 2CO + 2H_2 \qquad \Delta H^0_{298} = 247\ \text{kJ mol}^{-1}, \tag{2}$$

$$CH_4 + \tfrac{1}{2}O_2 \rightarrow CO + 2H_2 \qquad \Delta H^0_{298} = -36\ \text{kJ mol}^{-1}. \tag{3}$$

To achieve a process requiring less energy input than CO_2 reforming, Ashcroft et al. [5] suggested to combine the catalytic partial oxidation and CO_2 reforming of methane. They found that Al_2O_3-supported Ir catalysts were active for the combined reaction. Other groups carried out similar combination reactions by coupling the methane partial oxidation with CO_2 or H_2O reforming and using various catalysts [26–28]. The combined reactions have a number of advantages. Firstly, by coupling the exothermic partial oxidation reaction with the endothermic reforming reaction, the methane-to-syngas conversion can be operated in a safer manner than partial oxidation and more energy-efficient manner than CO_2 reforming. Secondly, by changing the feed composition, one can control the product ratio of H_2/CO and thus the selectivity for various Fischer–Tropsch synthesis products. Finally, one can use those natural gas reserves containing substantial amounts of CO_2.

Our previous research has shown that the Co/MgO catalyst provided high and stable activities for CO_2 reforming of methane [29] and its partial oxidation [30]. In the present paper, the combined catalytic partial oxidation and CO_2 reforming of methane over the same catalyst was investigated. For comparison purposes, the Co/CaO and Co/SiO_2 catalysts were also employed.

2. Experimental

2.1. Catalyst preparation

The supported catalysts were prepared by impregnating the supports with aqueous solutions of $Co(NO_3)_2{\cdot}6H_2O$, followed by overnight drying at 110 °C. The samples were then calcined in the open air of a furnace for 8 h at 800 °C. The calcined catalysts are denoted as Co(O)/M_xO_y (M = Mg, Ca, and Si) and the catalysts reduced in H_2 as Co/MO. Co loading means wt% Co in the completely reduced catalyst; all the catalysts had a loading of 24 wt%.

* To whom correspondence should be addressed.

2.2. Catalytic reaction

All the catalysts were tested under atmospheric pressure in a fixed-bed vertical quartz reactor (ID 4 mm), which was located in a furnace. The reactor was operated in a down flow mode with the catalyst held on a quartz wool bed. Before reaction, the catalysts were reduced *in situ* in a H_2 flow (30 ml min^{-1}) by increasing the temperature from room temperature to 600 °C at a rate of 20 °C min^{-1} and from 600 to 900 °C at a rate of 10 °C min^{-1}, without holding at 900 °C. After reduction, feed gases with a C/O ratio of 1 were introduced into the catalyst bed at a flow rate of 35.0 ml min^{-1}. The reactants and products were analyzed with an on-line gas chromatograph equipped with a Porapak Q column. An ice-cold trap was set between the reactor exit and the GC sampling valve to remove the water formed during reaction. The yields to H_2 and CO are defined as

$$H_2 \text{ yield } (\%) = \frac{H_2 \times 100}{(2 \times CH_{4,\,in})},$$

$$CO \text{ yield } (\%) = \frac{CO \times 100}{(CH_{4,\,in} + CO_{2,\,in})},$$

where H_2 and CO represent the moles of H_2 and CO produced per unit time, and $CH_{4,\,in}$ and $CO_{2,\,in}$ the moles introduced per unit time.

The blank tests, carried out in a reactor free of catalyst, indicated that the yields to CO and H_2 were negligible.

2.3. Catalyst characterization

2.3.1. BET surface area and the exposed Co surface area

The BET surface area of the calcined catalysts was determined via nitrogen adsorption using a Micromeritics ASAP2000 instrument. All the samples were degassed at 200 °C for at least 5 h in high vacuum before measurement.

The exposed Co metal surface area of the reduced catalysts was determined via CO chemisorption at room temperature, assuming a 1/1 stoichiometry. In each experiment, 20.0 mg of catalyst were used, and its reduction was carried out as described in section 2.2. After reduction, the catalyst was purged with an ultrahigh purity helium flow (35 ml min^{-1}) at 900 °C for 0.25 h, and then the sample was cooled to room temperature. CO pulses (10 μl per pulse) in the carrier gas (He, 35 ml min^{-1}) were then passed over the reduced catalyst and the CO uptake in each pulse was monitored using a thermal conductivity detector (TCD).

2.3.2. CH_4 decomposition

The decomposition of pure methane over the reduced catalyst was carried out in a pulse microreactor. In each experiment, 20.0 mg of catalyst was used, and its reduction was carried out as described previously. After reduction, the catalyst was purged with He (35 ml min^{-1}) at 900 °C for 0.25 h and then pulses of CH_4 (250 μl) were injected in the carrier gas He (35 ml min^{-1}). The products were analyzed with an on-line gas chromatograph equipped with a TCD and a Porapak Q column.

2.3.3. Temperature-programmed reduction (TPR)

During each TPR run, a high-purity 2.5% H_2/Ar mixture (35 ml min^{-1}), which was additionally purified using Hydro-Purge II and Oxy-Trap columns, was passed over a calcined sample (10.0 mg) in a vertical quartz tube reactor (ID 4 mm). The temperature of the sample was increased from 40 to 1000 °C, at a rate of 20 °C min^{-1}. The water, formed during reduction, was trapped in a Hydro-Purge II column. The hydrogen consumed in TPR was monitored continuously with a TCD, which was calibrated using known amounts of CoO and Co_3O_4.

2.3.4. X-ray powder diffraction (XRD)

A Siemens D500 X-ray diffractometer with monochromatized Cu Kα radiation was used for the X-ray determinations. The calcined catalysts were examined at a scanning rate of 1.2° min^{-1} and the obtained X-ray diffraction patterns were used to identify the major phases present.

3. Results

3.1. Combined partial oxidation and CO_2 reforming of methane to synthesis gas

3.1.1. Comparison of the catalysts supported on different supports

The combined reaction was carried out over the reduced Co/MgO, Co/CaO, and Co/SiO_2 catalysts at the high space velocity of 105 000 ml g^{-1} h^{-1} and at 900 °C with a feed gas of $CH_4/CO_2/O_2$ (4/2/1). The time-dependent conversions of CH_4, CO_2, and O_2 and yields to CO and H_2 are plotted in figure 1 (a)–(d). Over the Co/MgO catalyst, the conversions of CH_4 and CO_2 and yields to CO and H_2 increased somewhat during an activation period of about 18 h, after which they remained high (>90%) and unchanged during the period of study of 110 h (figure 1 (a), (b), and (d)). The conversion of O_2 was always 100% (figure 1(c)) and a H_2/CO ratio of about 1.40 was obtained. Over the Co/CaO and Co/SiO_2 catalysts, the CH_4 conversion was below 15% and the CO_2 conversion was negative (figure 1 (a) and (b)), indicating that some CO_2 was generated during reaction. Because no H_2 and CO were formed and the conversion of O_2 was roughly eight times that of CH_4 at a given time on stream (figure 1 (a) and (c)), it is obvious that only combustion of methane occurred over the two catalysts. In summary, the CaO- and SiO_2-supported catalysts provided no activity for the formation of H_2 and CO, while the MgO-supported catalyst provided 94–95% yields to H_2 and CO with high stability.

3.1.2. Effect of reaction temperature on the Co/MgO catalysts

The effect of temperature on the steady-state activity of Co/MgO and the product H_2/CO ratio is examined in figure 2. Only the CO yield is presented because the conversions of CH_4 and CO_2 and the H_2 yield followed the same

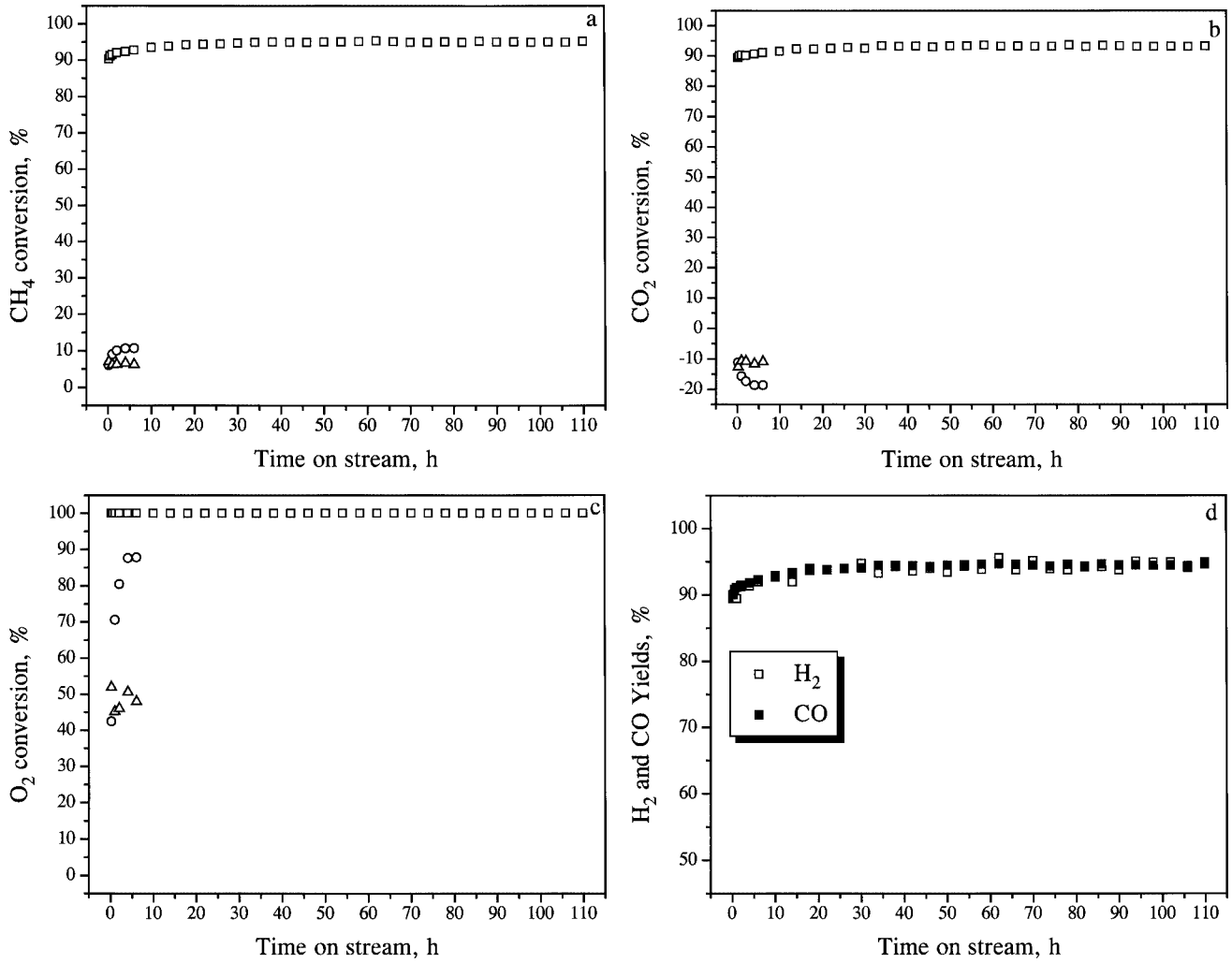

Figure 1. Time-dependent conversions of CH_4 (a), CO_2 (b) and O_2 (c), and yields to H_2 and CO (d) over Co/MgO (□), Co/CaO (○), and Co/SiO_2 (△). $P = 1$ atm, $T = 900\,^{\circ}$C, amount of catalyst = 20.0 mg, $CH_4/CO_2/O_2 = 4/2/1$, space velocity = 105 000 ml h^{-1} g^{-1}.

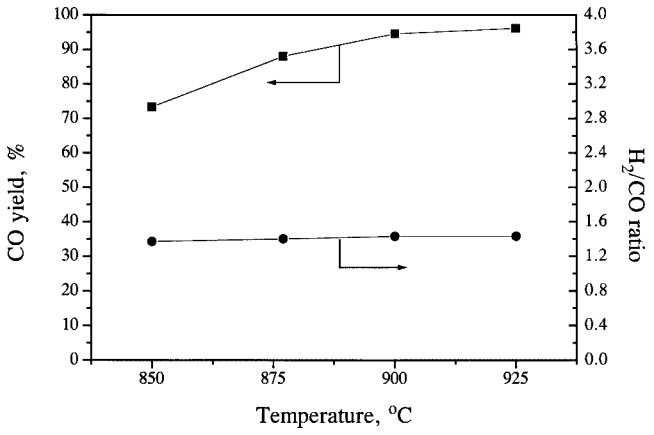

Figure 2. CO yield and H_2/CO ratio as a function of temperature over the Co/MgO catalyst. $P = 1$ atm, amount of catalyst = 20.0 mg, $CH_4/CO_2/O_2 = 4/2/1$, space velocity = 105 000 ml h^{-1} g^{-1}.

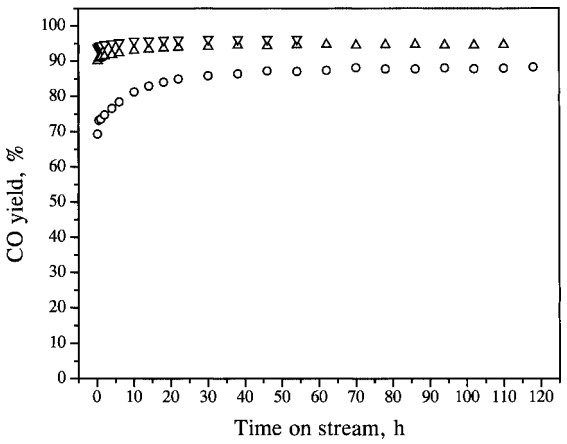

Figure 3. Time-dependent CO yield over the Co/MgO catalyst at various temperatures: (○) 877, (△) 900, and (▽) 925 °C. $P = 1$ atm, amount of catalyst = 20.0 mg, $CH_4/CO_2/O_2 = 4/2/1$, space velocity = 105 000 ml h^{-1} g^{-1}.

pattern. Clearly, the CO yield increased monotonically with increasing temperature, while the H_2/CO ratio remained almost unchanged at about 1.40.

The time-dependent CO yields at various temperatures are plotted in figure 3. An activation period was observed, which lasted longer at the lower temperatures.

3.1.3. Effect of space velocity on the MgO-supported Co catalysts

The space velocity was varied by changing the amount of catalyst while maintaining the total flow rate at 35.0 ml min^{-1}. The effect of space velocity on the steady-state activity of Co/MgO and the product H_2/CO ratio is presented in figure 4. Again, only the CO yield is plotted because the conversions of CH_4 and CO_2 and the H_2 yield followed the same pattern. With increasing space velocity, the CO yield notably decreased, the decrease being smaller at low space velocities. The equilibrium at the exit was achieved for space velocities lower than about 50 000 ml g^{-1} h^{-1}. The H_2/CO ratio obtained for space velocities $\leqslant$105 000 ml g^{-1} h^{-1} was slightly higher than that for space velocities $\geqslant$210 000 ml g^{-1} h^{-1}.

The time-dependent CO yields obtained for various space velocities are plotted in figure 5. Activation periods were observed for space velocities $\geqslant$105 000 ml g^{-1} h^{-1}. The higher the space velocity, the longer was the activation period.

3.1.4. Effect of O_2/CO_2 ratio

The effect of the O_2/CO_2 ratio was investigated for a C/O ratio of 1 and a total flow rate of 35.0 ml min^{-1} for the gas compositions listed in table 1. The effect of the O_2/CO_2 ratio on CO yield and H_2/CO ratio is presented in figure 6. The CO yield increased notably with increasing O_2/CO_2 ratio from 0 to 0.5, but remained almost unchanged with a further increase in the O_2/CO_2 ratio. The H_2/CO ratios obtained in the CO_2 reforming of methane (in the absence of O_2) and in the partial oxidation of methane (in the absence of CO_2) were around 1.0 and 2.0, respectively. The combined partial oxidation and CO_2 reforming of methane can provide a synthesis gas with a H_2/CO ratio between 1 and 2, which increases with increasing O_2/CO_2 ratio.

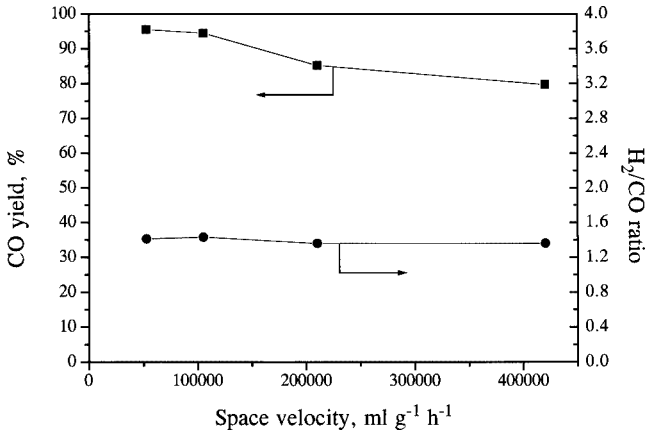

Figure 4. CO yield and H_2/CO ratio as a function of space velocity over the Co/MgO catalyst. $P = 1$ atm, $T = 900\,^{\circ}C$, $CH_4/CO_2/O_2 = 4/2/1$.

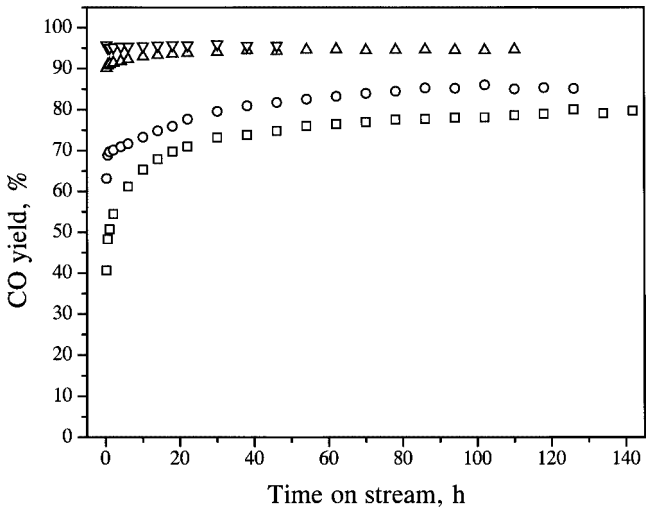

Figure 5. Time-dependent CO yield over the Co/MgO catalyst at various space velocities: (□) 420 000, (○) 210 000, (△) 105 000, (▽) 52 500 ml h^{-1} g^{-1}. $P = 1$ atm, $T = 900\,^{\circ}C$, $CH_4/CO_2/O_2 = 4/2/1$.

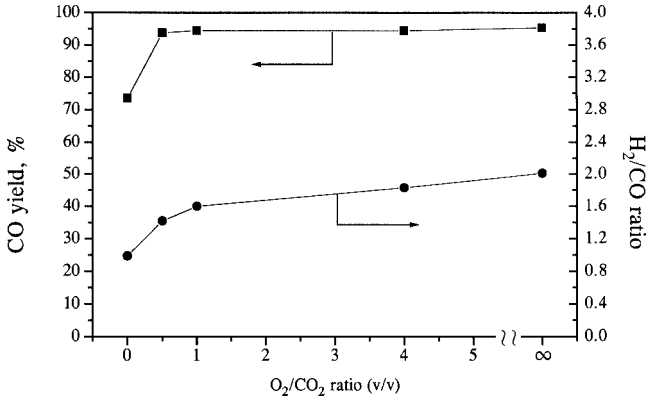

Figure 6. CO yield and H_2/CO ratio as a function of O_2/CO_2 ratio over the Co/MgO catalyst (data obtained after 22 h of reaction). $P = 1$ atm, $T = 900\,^{\circ}C$, amount of catalyst = 20.0 mg, $CH_4/(CO_2 + 2O_2) = 1/1$, space velocity = 105 000 ml h^{-1} g^{-1}.

Table 1
Various flow compositions used to investigate the effect of gas composition on the catalyst activity at 900 °C.

Test no.	CH_4 (ml min^{-1})	CO_2 (ml min^{-1})	O_2 (ml min^{-1})	Total (ml min^{-1})	$CH_4/(CO_2 + 2O_2)$ (v/v)	O_2/CO_2 (v/v)
1	17.5	17.5	0.0	35.0	1.0	0.0
2	20.0	10.0	5.0	35.0	1.0	0.5
3	21.0	7.0	7.0	35.0	1.0	1.0
4	22.5	2.5	10.0	35.0	1.0	4.0
5	23.3	0.0	11.7	35.0	1.0	∞

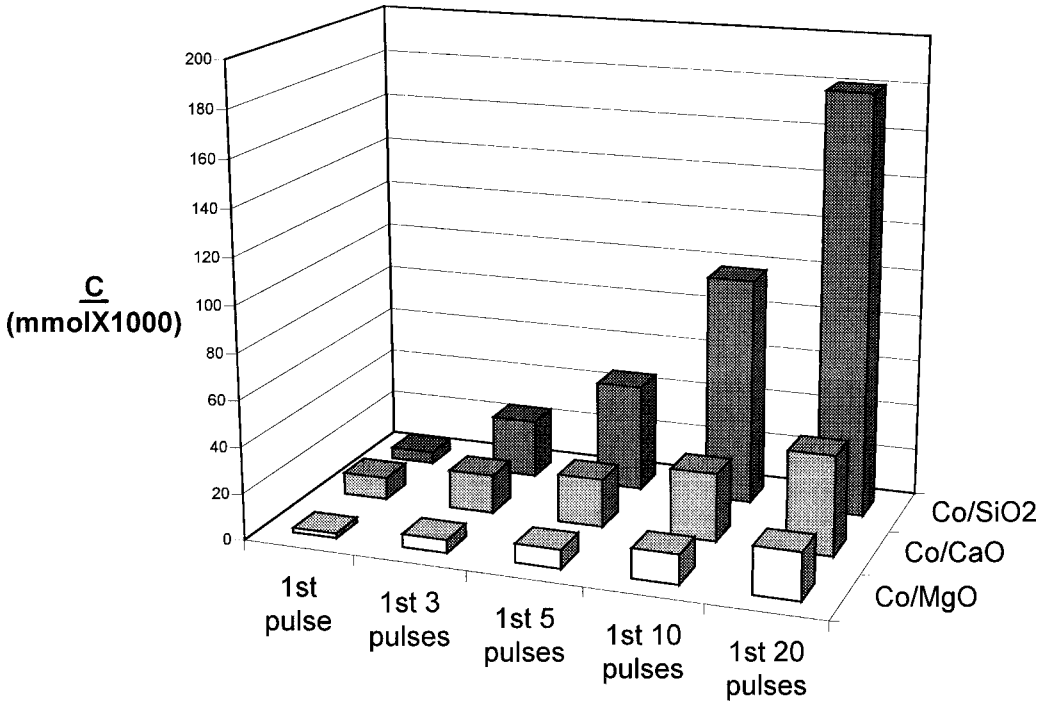

Figure 7. Amount of carbon (C) deposited during CH_4 decomposition over the reduced catalysts at 900 °C.

Table 2
Physical data for the supported Co (24 wt%) catalysts pre-calcined at 800 °C.

Support	Surf. area[a] (m^2 g-cat^{-1})	Co surf. area[b] (m^2 g-cat^{-1}) × 100
MgO	20	13
CaO	5	48
SiO_2	382	72

[a] For the calcined catalysts.
[b] For the reduced catalysts.

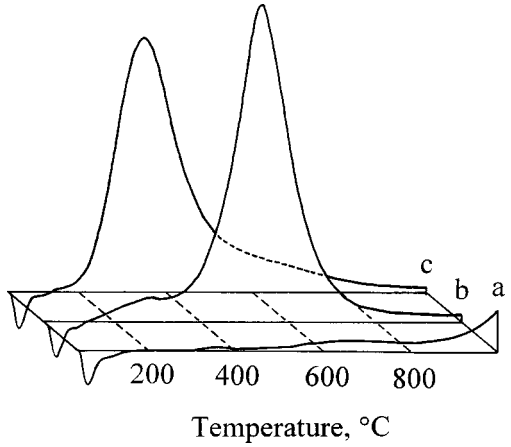

Figure 8. TPR profiles of calcined Co (24 wt% loading) catalysts supported on MgO (a), CaO (b), and SiO_2 (c).

3.2. Physico-chemical characterization

3.2.1. Exposed metallic Co surface area of the reduced catalyst

The exposed metallic Co surface area was determined after the catalyst was reduced under the conditions used in the catalytic runs. As shown in table 2, the exposed metal surface area of the reduced catalysts decreased in the sequence $SiO_2 > CaO > MgO$.

3.2.2. Surface carbon (C) formed in the CH_4 decomposition

The decomposition of CH_4 pulses over the reduced catalysts was carried out at 900 °C and the amount of surface carbon (C) generated was determined from the carbon balance. Figure 7 shows that the amount of C accumulated during the same period over Co/MgO was much lower than those over Co/CaO and Co/SiO_2.

3.2.3. Reduction characteristics of the calcined supported Co catalysts

The TPR spectra of the 800 °C calcined Co catalysts supported on various supports are plotted in figure 8. For Co(O)/MgO, a peak started to form at a temperature higher than 800 °C (figure 8(a)). A single peak at about 540 °C was observed for Co(O)/CaO (figure 8(b)), and a single peak at about 345 °C for Co(O)/SiO_2 (figure 8(c)). The extent of reduction of the MgO-supported catalyst after TPR was estimated to be below 5%, while nearly 100% reduction was reached for the CaO- and SiO_2-supported catalysts.

3.2.4. Compounds present in the calcined supported Co catalysts

By combining the XRD and TPR results, the major Co-containing species present in the calcined catalysts could be identified. The data and the assignments of the XRD patterns for the 800 °C calcined catalysts are listed in table 3. For the Co(O)/MgO, the XRD patterns could be attributed

Table 3
Data and assignments of XRD patterns of the 800 °C calcined supported Co (24 wt% loading) catalysts.

Catalyst	d (Å)	Assignment
24% Co(O)/MgO	2.106, 1.490, 1.269, 1.214, 2.431	(Co, Mg)O and/or MgO
24% Co(O)/CaO	2.686, 2.273, 3.587, 2.406, 2.083, 1.878	$Ca_3Co_4O_9$
24% Co(O)/SiO_2	2.435, 1.427, 1.555, 2.861, 2.028	Co_3O_4

to a solid solution of CoO and MgO (denoted as (Co, Mg)O) and/or MgO. The TPR spectrum (figure 8(a)), which exhibited a reduction peak that started to form at a temperature higher than 800 °C, allowed us to conclude that a solid solution was formed. $Ca_3Co_4O_9$ was identified over Co(O)/CaO, in agreement with the TPR spectrum (figure 8(b)) which provided a single reduction peak. Finally, over Co(O)/SiO_2, Co_3O_4 was identified, in agreement with the TPR spectrum which exhibited a single peak at about 345 °C (figure 8(c)).

4. Discussion

Among the catalysts investigated in the present paper, only Co/MgO provided a high and stable activity during the period of study of 110 h; the Co/CaO and Co/SiO_2 provided no activity for the formation of the synthesis gas. A correlation can be made among the species present in the calcined catalysts, their reduction behavior, and the catalytic performance of the reduced catalysts.

Firstly, the species formed in Co catalysts were closely dependent on the nature of the support. MgO and CaO have the same NaCl type structure as CoO. However, only MgO has a lattice parameter and bond distance close to CoO [31]; for this reason, a solid solution of CoO and MgO was generated in the MgO-supported catalyst after calcination at 800 °C (table 3). While a compound, $Ca_3Co_4O_9$, was identified in the CaO-supported catalyst, no compound was generated between cobalt oxide and SiO_2 and in the SiO_2-supported catalyst cobalt was present as Co_3O_4 (table 3).

Secondly, the Co-containing species present in the catalyst controlled its reducibility and the size and morphology of the metal particles generated during reduction. For the three Co-containing species, their reducibility increased in the sequence: (Co, MgO)O $\ll$ $Ca_3Co_4O_9$ < Co_3O_4 (figure 8). Due to the strong interactions between CoO and MgO, the solid solution was the most difficult to reduce. For this reason, the extent of reduction of the MgO-supported catalyst after the TPR run was below 5%, while a nearly 100% reduction was reached for the CaO- and SiO_2-supported catalysts (estimated on the basis of figure 8). Similarly, after reduction under the conditions used in the catalytic runs, the smallest exposed Co surface area was obtained over the MgO-supported catalyst (table 2). The size of the metal clusters in the reduced catalyst was strongly affected by the reducibility of the catalyst. The higher the reducibility, the larger is expected to be the size of the metal particles. As already revealed by XRD and TPR, in the MgO-supported catalyst, a solid solution of (Co, Mg)O, which is much less reducible than $Ca_3Co_4O_9$ and Co_3O_4, was generated (table 3 and figure 8). Thus, the size of the metal clusters is expected to be small for the MgO-supported catalyst. Parmaliana et al. brought transmission electron microscopy (TEM) evidence for a quasi-uniform distribution of small Ni particles (d = 25 Å) originated through the reduction of Ni^{2+} ions dispersed in the MgO matrix of a NiO–MgO solid solution [32]. Moreover, due to the low reducibility of the solid solution, its reduction was limited to few surface layers only. During reduction, some Co^0 atoms formed fine metal particles exposed to the chemical atmosphere, while others, which lay deeper, were present in the MgO matrix either as Co^0 or mostly as Co species in a low oxidation state. Being extracted from the substrate, the generated metallic clusters were partially embedded into the MgO lattice. Parmaliana et al. brought TEM evidence that such embedding was present in the reduced NiO–MgO solid solution systems [32].

Finally, the surface features of the generated metallic particles controlled the catalytic pattern of a catalyst. The carbon deposition and the metal sintering constitute the main causes for catalyst deactivation in the methane conversion reactions, which are usually carried out at high temperatures (>800 °C). Sintering decreased not only the number of active sites, but also accelerated the carbon deposition, since large metal ensembles stimulate coke formation [33]. As already mentioned, the metallic crystallites generated over the MgO-supported catalyst were small and partially embedded into the lattice of MgO. Being small, the carbon deposition could be suppressed. Indeed, as shown in figure 7, the carbon deposition during the decomposition of pure CH_4 was much lower over MgO than over CaO and SiO_2. Being partially embedded into the MgO lattice, they became more resistant to sintering than the crystallites supported on the conventional supports [34]. For these reasons, the Co/MgO provided a high and stable activity for the combined partial oxidation and CO_2 reforming of methane. As already noted, $Ca_3Co_4O_9$ and Co_3O_4 are much more reducible than the solid solution of CoO and MgO (figure 8). For this reason, larger exposed Co surface areas were obtained after reduction over CaO and SiO_2 than over MgO (table 2). However, the former two provided no activity for the formation of synthesis gas, but some activity for combustion. This most likely occurred because of the generation of large metallic particles during reduction, which stimulated carbon deposition. Consequently, too few metallic sites remained accessible for the formation of H_2 and CO. In conclusion, the high stability of the Co/MgO catalyst is due to the formation of a solid solution between CoO and MgO after a high-temperature calcination.

The reaction temperature and space velocity exert significant influences on the activity of Co/MgO catalysts, and the O_2/CO_2 ratio of the feed gases a significant effect on the H_2/CO ratio. As expected, the steady-state CO yield

increased with increasing reaction temperature (figure 2) and decreased with increasing space velocity from 52 500 to 420 000 ml g^{-1} h^{-1} (figure 4). In the partial oxidation of methane [35], the CH_4 conversion remained unchanged (at about 85%) with increasing space velocity from 180 000 to 720 000 ml g^{-1} h^{-1} because of the presence of hot spots. For the endothermic CO_2 reforming of methane over the Co/MgO catalyst, the reaction had to be operated at a low space velocity ($\leqslant$60 000 ml g^{-1} h^{-1}) to reach high (>90%) yields to H_2 and CO [29]. In contrast, for the combined reaction, high yields (about 85%) could be reached even at the high space velocity of 210 000 ml g^{-1} h^{-1} (figures 4 and 5). Hot spots, less bright than in the partial oxidation of methane, have been observed visually during the combined reaction. Consequently, the combined reaction can be operated in a more efficient manner than the CO_2 reforming and in a safer manner than the partial oxidation. The H_2/CO product ratio in the combined reaction increased with increasing O_2/CO_2 ratio in the feed (figure 6). Thus, by changing the O_2/CO_2 ratio one can control the product H_2/CO ratio within a range between 1 and 2, values which correspond to the H_2/CO ratio in the CO_2 reforming of methane and the partial oxidation of methane, respectively. Activation periods were noted for temperatures $\leqslant$900 °C (figure 3) and space velocities $\geqslant$105 000 ml g^{-1} h^{-1} (figure 5), that lasted longer at lower temperatures (figure 3) and larger space velocities (figure 5). These results indicate that additional metallic sites were generated during reaction via the reduction of the unreduced solid solution by CH_4 and/or H_2 until a steady state was achieved. Consequently, the solid solution catalyst acted like a "reservoir" which provided additional active metallic sites during reaction. This constitutes an additional positive feature of the solid solution catalyst. Of course, additional active sites were also generated at the low space velocity of 52 500 ml g^{-1} h^{-1}, for which no activation period was noted (figure 5). However, in that case, the initial number of sites was sufficient to achieve thermodynamic equilibrium at the exit of the reactor.

5. Summary

The following conclusions can be drawn regarding the combined catalytic partial oxidation and CO_2 reforming of methane over supported Co catalysts:

(1) After a high-temperature calcination, a solid solution of CoO and MgO, $Ca_3Co_4O_9$, and Co_3O_4 were formed in the MgO-, CaO-, and SiO_2-supported catalysts, respectively. The species present in the calcined catalyst had a significant effect on its reduction behavior and catalytic performance.

(2) The reduced Co/MgO catalyst exhibited a high and stable activity for the combined reaction, while the Co/CaO and Co/SiO_2 provided no activity for the formation of synthesis gas.

(3) By changing the O_2/CO_2 ratio of the feed gases one could control the product H_2/CO ratio between 1 and 2.

References

[1] J.R. Rostrup-Nielsen, Catal. Today 18 (1993) 305.
[2] J.M. Fox, III, Catal. Rev. Sci. Eng. 35 (1993) 169.
[3] A.M. Gadalla and B. Bower, Chem. Eng. Sci. 43 (1988) 3049.
[4] J.T. Richardson and S.A. Paripatyadar, Appl. Catal. 61 (1990) 293.
[5] A.T. Ashcroft, A.K. Cheetham, M.L.H. Green and P.D.F. Vernon, Nature 352 (1991) 225.
[6] J.R. Rostrup-Nielsen and J.-H.B. Hansen, J. Catal. 144 (1993) 38.
[7] E. Ruckenstein and Y.H. Hu, Appl. Catal. A 133 (1995) 149.
[8] V.C.H. Kroll, H.M. Swaan and C. Mirodatos, J. Catal. 161 (1996) 409.
[9] R.N. Bhat and W.M.H. Sachtler, Appl. Catal. A 150 (1997) 279.
[10] S.M. Stagg, E. Romeo, C. Padro and D.E. Resasco, J. Catal. 178 (1998) 137.
[11] K. Tomishige, Y. Chen and K. Fujimoto, J. Catal. 181 (1999) 91.
[12] H.Y. Wang and E. Ruckenstein, Appl. Catal. A 204 (2000) 143.
[13] A.T. Ashcroft, A.K. Cheetham, J.S. Foord et al., Nature 344 (1990) 319.
[14] D. Dissanayake, M.P. Rosynek, K.C.C. Kharas and L.H. Lunsford, J. Catal. 132 (1991) 117.
[15] D.A. Hickman and L.D. Schmidt, J. Catal. 138 (1992) 267.
[16] D.A. Hickman and L.D. Schmidt, Science 259 (1993) 343.
[17] A. Slagtern and U. Olsbye, Appl. Catal. A 110 (1994) 99.
[18] V.R. Choudhary, B.S. Uphade and A.S. Mamman, Catal. Lett. 32 (1995) 387.
[19] A. Santos, M. Menéndez, A. Monzón et al., J. Catal. 158 (1996) 83.
[20] R. Lago, G. Bini, M.A. Pena and J.L.G. Fierro, J. Catal. 167 (1997) 198.
[21] V.A. Tsipouriari, Z. Zhang and X.E.J. Verykios, J. Catal. 179 (1998) 283.
[22] E. Ruckenstein and Y.H. Hu, Appl. Catal. A 183 (1999) 85.
[23] E. Ruckenstein and H.Y. Wang, J. Catal. 187 (1999) 151.
[24] D. Dissanayake, M.P. Rosynek and J.H. Lunsford, J. Phys. Chem. 97 (1993) 3644.
[25] Y.F. Chang and H. Heinemann, Catal. Lett. 21 (1993) 215.
[26] V.R. Choudhary, B.S. Uphade and A.A. Belhekar, J. Catal. 163 (1996) 312.
[27] A.M. O'Connor and J.R.H. Ross, Catal. Today 46 (1998) 203.
[28] E. Ruckenstein and Y.H. Hu, Ind. Eng. Chem. Res. 37 (1998) 1744.
[29] E. Ruckenstein and H.Y. Wang, Appl. Catal. A 204 (2000) 257.
[30] H.Y. Wang and E. Ruckenstein, J. Catal. (2001), in press.
[31] I. Náray-Szabó, *Inorganic Crystal Chemistry* (Akadémiai Kiadó, Budapest, 1969) p. 237.
[32] A. Parmaliana, F. Arena, F. Frusteri et al., J. Catal. 141 (1993) 34.
[33] J.R. Rostrup-Nielsen, in: *Catalysis Science and Technology*, Vol. 5, eds. J.R. Anderson and M. Boudart (Springer, Berlin, 1984) pp. 1–118.
[34] J.G. Highfield, A. Bossi and F.S. Stone, Stud. Surf. Sci. Catal. 16 (1983) 181.
[35] E. Ruckenstein and H.Y. Wang, Appl. Catal. A 198 (2000) 33.